JCIM JOURNAL OF CHEMICAL INFORMATION AND MODELING

pubs.acs.org/jcim Article

3-Input AND Molecular Logic Gate with Enhanced Fluorescence Output: The Key Atom for the Accurate Prediction of the Spectra

Christina Eleftheria Tzeliou and Demeter Tzeli*

Cite This: J. Chem. Inf. Model. 2022, 62, 6436−6448 Read Online

ACCESS | Metrics & More | Article Recommendations | Supporting Information

ABSTRACT: The development of artificial receptors for sensing and recognition of species, as well as for advanced logic functions, is a significant challenge in the field of molecular information technology. Here, we study theoretically, via DFT/TD-DFT calculations, the photophysical properties of a 3-input AND molecular logic gate which presents an enhanced fluorescence spectrum. It was found that the geometry conformation at an N atom of the piperazine group is the key factor for the correct calculation of the absorption spectra of the calculated structures. Its geometry is between tetrahedral and planar, while changes in the corresponding CNCC dihedral angle of about 10 degrees can cause significant shifts of the main peak of the absorption spectra up to 100 nm. Moreover, the unusually enhanced fluorescence of a molecular logic gate (MLG) is explained. Finally, we conclude that molecular systems having N atoms, whose geometry is between planar and tetrahedral, can be ideal molecules as sensors and molecular logic gates. Our calculated absorption and emission spectra are in excellent agreement with available experimental data.

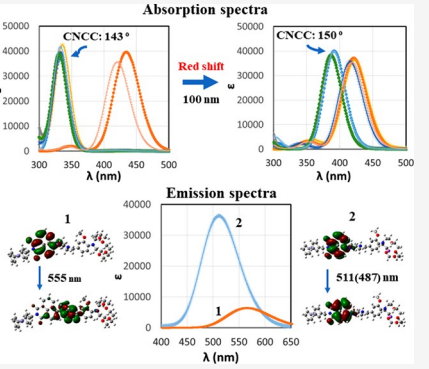

I. INTRODUCTION

The ability of molecules to process information similar to electronic systems was first demonstrated in 1993 by de Silva.[1] His idea was based on the explicit "off−on" fluorescence response of Photoinduced Electron Transfer-based chemosensors in response to the addition of metal ions.[1] Since then, artificial receptors for sensing and recognition of environmentally and biologically important ionic species have been designed, as well as molecular systems that exhibit sequential advanced logic functions.[2−9] The design of the last ones is a significant challenge in the field of molecular information technology.[5] It is of interest that a molecular logic gate (MLG) can process modulators incorporating different logic gates on the same molecule. Such a function is called integrated logic, and it is not found in conventional logic gates (electronic devices).[5,10]

The development of sensors and MLG is of great interest in many fields of science as biological probes, environmental sensors, and molecular devices,[2−9] while chemistry has a crucial role in the controlled design of molecular and supramolecular structures, which can be addressed by external stimuli (input), and it can produce one or more answer signals (output).[4] Usually, these molecular systems can be designed according to the principles of modular photoelectron transfer in a 'fluorophore−spacer−receptor' or 'fluorophore−spacer−receptor1−spacer−receptor2' format. Their absorption and emission spectra can be modulated by different combinations of external input, such as light, metal ions, anions, solution pH, and solvent polarity.[2] Finally, a necessary requirement for a molecular system to be used as a molecular logic gate[11] is that it has to exist in at least two thermally stable forms (states), which differ by properties and which can be converted from one to another by some external stimulus.[5,9,12,13]

Up to now, various 3-input AND molecular logic gates have been developed and examined for different applications both experimentally and theoretically [see, for instance, refs 5 and 12−22]. Recently, a 3-input AND molecular logic gate (**1**) which presents the largest fluorescence enhancement to date was synthesized. Molecule **1** is devised in a modular format according to the principles of photoinduced electron transfer systems, see Scheme 1. The molecule has been synthesized,[17] and it has been proved experimentally that it detects three cations by three different titrimetric methods: H^+ by acid−base chemistry, Na^+ by complexation, and Fe^{3+} by redox chemistry. Molecule **2** has a high fluorescence "on" state when all three inputs are at the same time present in aqueous methanol solution, while the remaining seven possible input conditions result in a quenching of the emission.

Here, we investigate theoretically the photophysical processes of the forementioned system where all eight species involved in the logical operation are studied. The unusually enhanced fluorescence of **2** is explained, and the requirements

Special Issue: Advancing Women in Chemistry

Received: March 3, 2022
Published: April 19, 2022

https://doi.org/10.1021/acs.jcim.2c00257
J. Chem. Inf. Model. 2022, 62, 6436−6448

Scheme 1. Calculated Species of 3-Input AND MLG 1 and Its Product 2

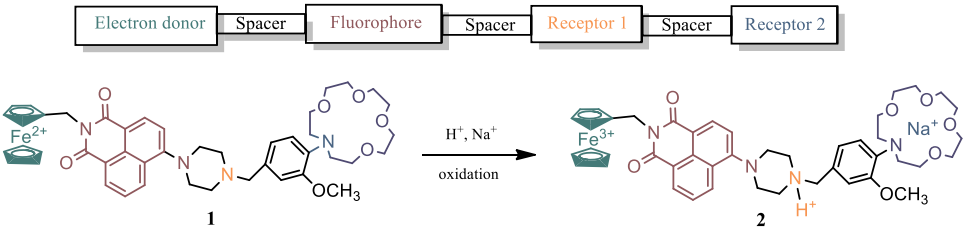

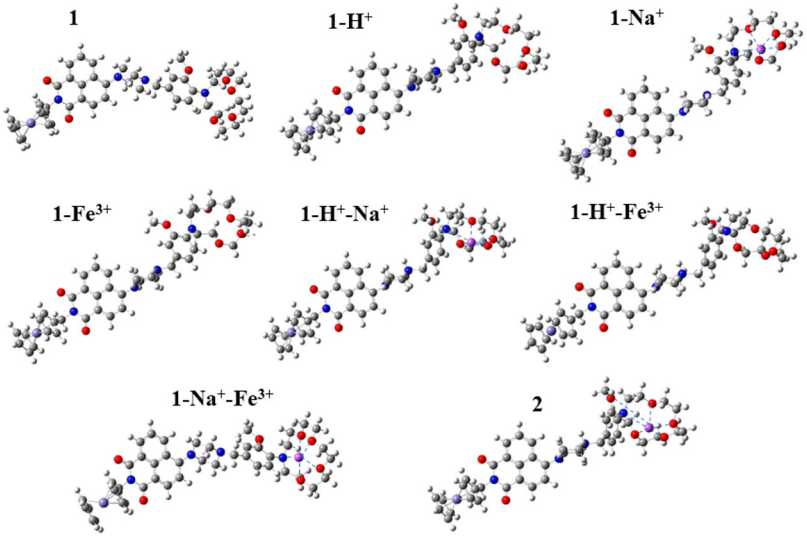

Figure 1. Minimum calculated structures of **1**, **1-M**, **1-M1-M2**, and **2** at PBE0/6-31G(d,p). The water solvent is included implicitly.

Table 1. Selected Distances (Å) and Dihedral Angles (deg) of the Calculated Structures Including Solvent Implicitly

molecule	R_1[a]	R_2[a]	R_{Na-O}	R_{Na-N}	d_1[b]	d_2[c]	d_3[c]	d_4[c]	d_5[c]
1	1.622	1.620			32.83	179.48	151.14	125.06	168.57
1-H$^+$	1.622	1.617			30.76	178.40	143.52	125.74	177.16
1-Na$^+$	1.626	1.620	2.365−2.458	2.709	34.81	178.73	141.99	125.03	142.05
1-Fe^{3+}	1.643	1.641			32.90	177.98	141.92	124.63	168.48
1-Na$^+$-Fe^{3+}	1.640	1.648	2.341−2.442	2.600	36.52	179.48	158.83	125.45	145.75
1-H$^+$-Na$^+$	1.622	1.620	2.366−2.446	2.858	32.03	178.55	143.40	125.48	147.78
1-H$^+$-Fe^{3+}	1.714	1.707			31.08	178.29	145.52	126.42	150.00
2 (**1-H$^+$-Na$^+$-Fe^{3+}**)	1.642	1.641	2.366−2.437	2.821	32.50	178.39	143.37	126.19	146.77

[a]R_1 and R_2: the R distance of Fe from the center of each cyclopentadienyl ring in the ferrocene unit; R_1 corresponds to the outer ring, and R_2 refers to the ring connected to the pyridine group. [b]Dihedral OOOO angle. [c]Dihedral CNCC angles of pyridine (d_2), piperazine (d_3: toward ferrocene; d_4: toward azacrown ether), and azacrown ether (d_5), i.e., dihedral angles of the N atom and its nearby connected C atoms.

for systems that may have this enhancement are reported. Additionally, emphasis is given here to find the key factors for the accurate prediction of the spectra, given that, in some cases, theoretical calculations predict spectra significantly red- or blue-shifted, with respect to experimental ones. The need for the explicit inclusion of the solvent effect and the special characteristics that molecules may have so as to have potential applications as sensors and molecular logic gates are investigated.

II. COMPUTATIONAL DETAILS

We have studied via density functional theory (DFT) and time-dependent DFT (TD-DFT) the electronic structure of molecule **1**, its monometallic complexes, **1-M**, with M = H$^+$, Na$^+$, and Fe^{3+}, that is, **1-H$^+$**, **1-Na$^+$**, and **1-Fe^{3+}**, the bimetallic complex of **1** with all possible combinations of the cations, **1-M1-M2**, that is, **1-H$^+$-Na$^+$**, **1-H$^+$-Fe^{3+}**, and **1-Na$^+$-Fe^{3+}**, and the trimetallic complex of **1** with all three cations, **2**, see Scheme 1. The calculations were carried out using the PBE0[23] and B3LYP[24] functionals in conjunction with the 6-31G(d,p)[25] basis set. Conformational analyses were carried out at first. All species were fully geometry optimized in the ground state and for some excited states of interest as well. All calculations were carried out in the water solvent employing the polarizable continuum model (PCM).[26] This model is divided into a solute part lying inside a cavity, surrounded by the solvent part represented as a material without structure, characterized by its macroscopic properties, i.e., dielectric constants and solvent radius. Finally, in addition to the implicit inclusion of the solvent via a dielectric constant, one molecule of the water solvent has been added explicitly to all calculated species. Furthermore, in order to check the influence of the addition of more water molecules than one, three water molecules have been added to **1-Na$^+$** and **2** complexes.

https://doi.org/10.1021/acs.jcim.2c00257
J. Chem. Inf. Model. 2022, 62, 6436−6448

The absorption and emission spectra of the studied structures were calculated via the TD-DFT methodology in the water solvent. In all cases, the absorption and emission spectra of the studied systems were calculated including up to 40 singlet-spin excited electronic states. The Linear Response Correction (cLR) approach has been employed for the main absorption and emission peaks.[27] The change of the spectra due to explicit inclusion of the solvent is investigated.

It should be mentioned that the methodology used here has already been applied in similar systems, including complexes of azacrown ethers, for the calculation of the absorption and emission spectra[2,13,28] in good agreement with available experimental data.[15] Thus, the PBE0/6-31G(d,p) method is considered as a particularly good choice for this current study where the calculation of the absorption and emission spectra is of high importance for the correct prediction of a molecular system as a molecular logic gate.

All calculations were performed using the Gaussian 16[29] program package. The coordinates of all the optimum structures are included in the accompanying Supporting Information (SI).

III. RESULTS AND DISCUSSION

IIIA. Geometry. The calculated minimum structures of the eight species are depicted in Figure 1, and selected distances are presented in Table 1. It is of interest that the complexation of Na^+ or the oxidation of Fe^{2+} affects the geometry of remote groups. In the ferrocene unit, the bond distances between the iron cation and the center of the cyclopentadienyl ring, R_1 and R_2, differ by less than 0.01 Å in each species. For Fe^{2+} complexes, they are about 1.62 Å, while for Fe^{3+}, they are increased by about 0.02 Å, except for **1-H$^+$-Fe^{3+}**, where it is increased significantly by about 0.09 Å. Furthermore, in the azacrown ether, the $Na^+\cdots O$ distances range from 2.34 to 2.46 Å, while the $Na^+\cdots N$ distance depends strongly on the protonation of the piperazine or the oxidation of the Fe cation. The shortest $Na^+\cdots N$ distance is observed in **1-Na$^+$-Fe^{3+}**, i.e., 2.60 Å, and the most elongated one is found in **1-H$^+$-Na$^+$**, i.e., 2.86 Å, while in **1-Na$^+$**, it is 2.71 Å.

In the azacrown ether, the four oxygen atoms are not located in a plane; they form dihedral angles that range from 30.8 to 36.5 degrees. The complexation of Na^+ increases the OOOO dihedral angle by only 2 degrees, and the iron oxidation increases this angle by 4 degrees in total. However, the protonation of **1-Na$^+$** or the simultaneous protonation and the oxidation result in the same dihedral angle with that of **1**. Finally, we observe that the protonation of the piperazine in all cases, i.e., the protonation of **1**, **1-Na$^+$**, **1-Fe^{3+}**, and **1-Na$^+$-Fe^{3+}**, results in a smaller dihedral angle by 2 to 4 degrees, which is interesting given that the protonated atom is a remote group with respect to the azacrown ether.

Regarding the four N atoms, the N atom of pyridine has an almost planar geometry, i.e., the CNCC angle of pyridine is about 178 degrees (d_2 value of Table 1); on the contrary, the N atom of the piperazine next to the azacrown ether has an almost tetrahedral geometry (d_4 value of Table 1), i.e., this CNCC angle is about 125 degrees. The other two N atoms, namely the N atom of piperazine toward the ferrocene and the N atom of the azacrown ether, have intermediate values (from 142 to 169 degrees), with the exception of **1-H$^+$** where the N atom of the azacrown ether has a planar geometry. From the values obtained, we conclude that the molecule is planar in the part that is linked to the ferrocene and bent in the nitrogen that acts as a receptor for the H^+ cation. This is the reason why the N atom of the piperazine unit is easily protonated in acidic conditions and partially in aqueous solutions. Finally, the fact that the d_3 and d_5 CNCC angles which belong to fluorophore and receptor 2 (see Figure 1), respectively, have intermediate values between planar and tetrahedral geometry means that they are flexible, and they can be planar or tetrahedral in excited states. It has been demonstrated[13,30] that this flexibility is related to the quenching or not of the emission spectrum. For instance, a derivative of bodipy acts as a 3-input AND MLG because the emission is accomplished by only the simultaneous tetrahedral geometry of all three aniline N atoms which is achieved via the existence of the three metal dications attached to the three different receptors.[13] Another example is the pyramidalization of the nitrogen atom which corresponds to an emitted molecular structure, where a nearly planar conformation of N corresponds to the geometry of the charge transfer state and the emission is quenched.

Finally, in addition to the implicit inclusion of the water solvent, a water molecule was explicitly included. It was added next to the N atoms of piperazine (Scheme 2) from two

Scheme 2. Explicit Inclusion of Water Molecule from Two Different Directions

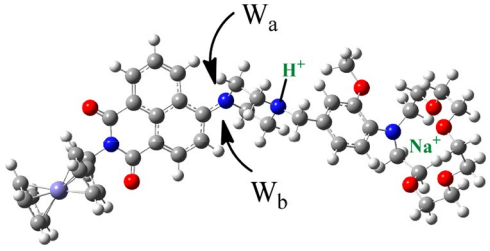

different positions (a and b) because this N atom presents a geometry between planar and tetrahedral. All structures were then fully optimized. In the first position, the W_a water molecule forms van der Waals bonds (i) with the N atom, HOH···N, that range from 1.623 (**2**) to 2.073 (**1-H$^+$-Fe^{3+}**); (ii) with the H of the phenyl group, $H_2O\cdots H$, with bond distances of about 2.5 Å with the exception of **2** (2.2 Å); and (iii) with weak $H_2O\cdots H$(of the CH_2 group) bonds with bond distances of about 2.6 Å with the exception of **2** (1.726 Å). In the second position, the W_b water molecule interacts with the phenyl group forming HOH···C weak interactions and with the H of CH_2 of piperazine forming $H_2O\cdots HCH<$ weak interactions with bond distances ranging from 2.27 to 2.90 Å. The calculated structures are shown in Figures 2 and 3, and selected geometric data are given in Table 2. Furthermore, for the **1-Na$^+$** and **2** complexes, the other two water molecules were added to the area next to the N atoms of pyridine and azacrown ether, i.e., in total, three water molecules have been added, see Figure 3, part II.

It is very interesting how the addition of the water molecule alters the geometry of all eight complexes. Even the remote groups change notably. Thus, the R_1 and R_2 bond distances of ferrocene differ significantly when the water molecule has been included explicitly. Now, they differ from 0.06 Å (**1-Na$^+$-Fe^{3+}**) to 0.35 Å (**1-H$^+$**), while when the water is included only implicitly, they differ less than 0.008 Å. Finally, for the structures where large differences are observed between R_1 and R_2, the elongated R is the R_2, i.e., the Fe - inner cyclopentadienyl ring distance, with the exception of **1-H$^+$**

https://doi.org/10.1021/acs.jcim.2c00257
J. Chem. Inf. Model. 2022, 62, 6436−6448

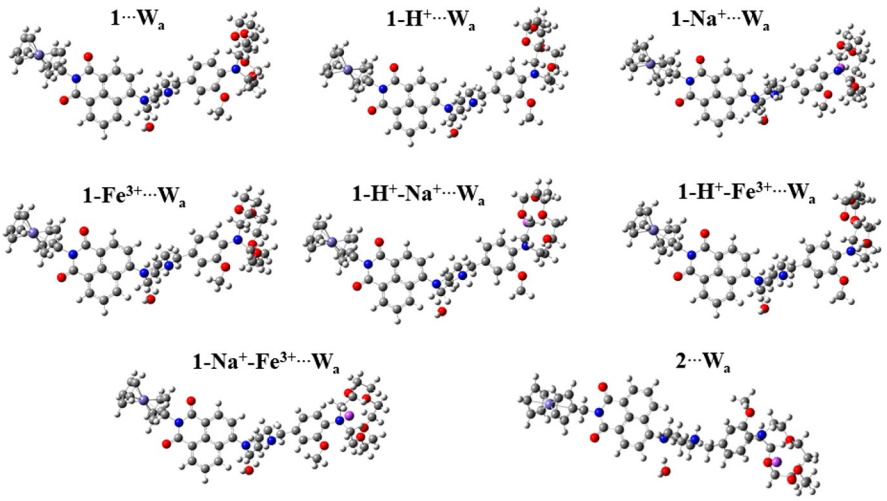

Figure 2. Minimum calculated structures of **1**, **1-M**, **1-M1-M2**, and **2**. Implicit addition of the water solvent and explicit inclusion of a water molecule from the "a" direction, see Scheme 2.

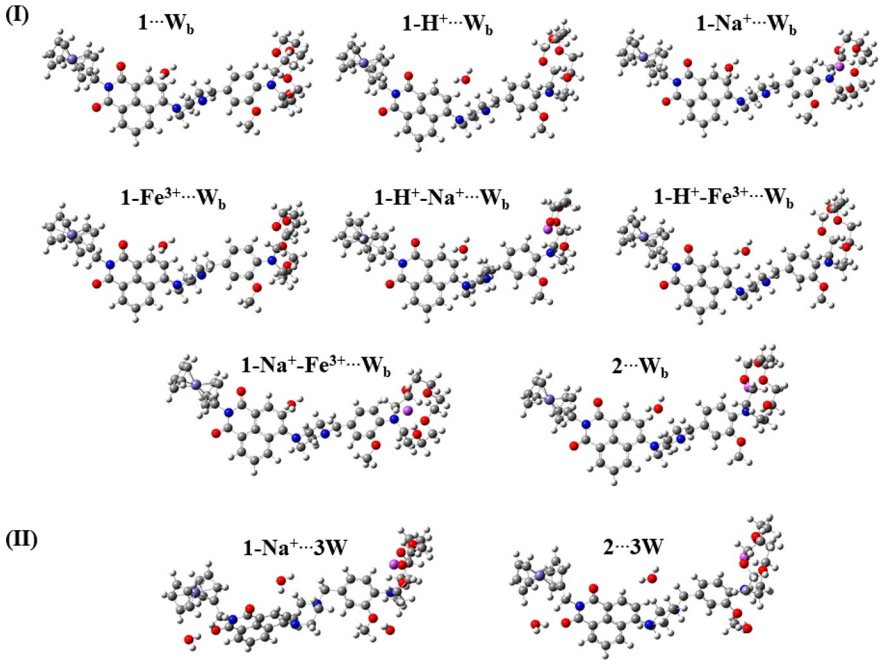

Figure 3. Minimum calculated structures of **1**, **1-M**, **1-M1-M2**, and **2**. (I) Implicit addition of the water solvent and explicit inclusion of a water molecule from the "b" direction, see Scheme 2. (II) Implicit addition of the water solvent and explicit inclusion of three water molecules.

where the R_1 is the elongated distance. The elongated distances mean that the corresponding cyclopentadienyl is less negatively charged than the other one, i.e., in **1-H$^+$**, the electron charge is located adjacent to the inner ring, while in the other cases. it is located adjacent to the outer cyclopentadienyl ring.

For the azacrown ether group, the inclusion of a water molecule changes the R_{Na-O} and R_{Na-N} distances only slightly; only in some cases, they are increased up to 0.02 Å, except for the R_{Na-N} distance of **1-Na$^+$-Fe^{3+}** which is elongated by 0.1 Å. Moreover, the OOOO dihedral angle is slightly decreased; the largest decrease is by 2 degrees for the **1-Na$^+$-Fe^{3+}** complex.

Regarding the four N atoms of the complexes, the inclusion of water does not change the geometry of the N atom of pyridine (d_2 value of Tables 1 and 2), i.e., it retains its planar geometry, while the N atom of the piperazine next to the azacrown ether maintains its tetrahedral geometry (d_4 value of Tables 1 and 2). The N atoms of the azacrown ether have intermediate values (from 142 to 177 degrees). The addition of water does not affect them, apart from **1-Na$^+$** and **1-H$^+$-Fe^{3+}** where the corresponding CNCC dihedral angles are increased by 23 degrees (W$_a$) and 27 degrees (W$_a$ and W$_b$), respectively. Finally, the N atoms of piperazine toward the ferrocene have intermediate values for the CNCC dihedral angles with respect to the tetrahedral and planar geometry. When the solvent is included only implicitly, i.e., they range from 142 to 159 degrees; however, the addition of the water molecule results in similar values for all complexes, i.e., about 141 degrees for W$_a$ and about 150 degrees for W$_b$. Finally, to check the influence of the addition of more water molecules than one, three water molecules have been added to **1-Na$^+$** and **2** complexes. It was found that the inclusion of additional water molecules to the **1-**

https://doi.org/10.1021/acs.jcim.2c00257
J. Chem. Inf. Model. 2022, 62, 6436−6448

Table 2. Selected Distances (Å) and Dihedral Angles (deg) of the Calculated Structures Including Solvent Implicitly and Explicitly

molecule	R_1[a]	R_2[a]	R_{Na-O}	R_{Na-N}	d_1[b]	d_2[c]	d_3[c]	d_4[c]	d_5[c]	R_{X-H}[d]	R_{O-H}[e]	R_{O-H}[f]
						Molecule··· W_a						
1	1.510	1.765			32.17	179.11	140.31	124.21	172.50	1.972	2.460	2.715
1-H$^+$	1.783	1.429			30.40	179.42	142.07	125.48	177.21	2.055	2.495	2.553
1-Na$^+$	1.550	1.797	2.365−2.467	2.706	34.57	179.32	140.90	124.64	165.50	1.977	2.468	2.694
1-Fe^{3+}	1.609	1.782			32.01	178.82	141.48	124.82	170.36	1.988	2.459	2.690
1-Na$^+$-Fe^{3+}	1.619	1.556	2.365−2.466	2.705	34.60	178.86	141.55	124.78	144.63	1.989	2.462	2.684
1-H$^+$-Na$^+$	1.497	1.726	2.368−2.447	2.870	31.57	179.39	142.23	125.33	150.44	2.062	2.496	2.544
1-H$^+$-Fe^{3+}	1.567	1.740			30.44	179.07	142.64	125.45	177.32	2.073	2.492	2.539
2	1.774	1.696	2.366−2.437	2.821	32.50	178.39	143.37	125.44	148.90	1.623	2.210	1.726
						Molecule··· W_b						
1	1.586	1.694			32.75	179.45	151.48	124.77	168.74	2.451		2.565
1-H$^+$	1.741	1.520			30.47	179.48	148.20	124.99	177.37	2.783		2.284
1-Na$^+$	1.486	1.675	2.366−2.465	2.703	34.69	179.44	150.66	124.97	142.47	2.575		2.708
1-Fe^{3+}	1.560	1.733			32.82	178.92	152.29	124.81	168.65	2.463		2.567
1-Na$^+$-Fe^{3+}	1.505	1.744	2.364−2.466	2.702	34.76	178.93	151.81	124.61	142.40	2.468		2.546
1-H$^+$-Na$^+$	1.565	1.759	2.365−2.451	2.842	32.48	179.28	148.35	125.01	146.76	2.857		2.266
1-H$^+$-Fe^{3+}	1.530	1.798			30.50	178.98	148.79	125.00	177.44	2.831		2.276
2	1.578	1.710	2.365−2.450	2.847	32.41	178.85	149.17	125.08	146.97	2.899		2.473

[a]R_1 and R_2: the R distance of Fe from the center of each cyclopentadienyl ring in the ferrocene unit; R_1 corresponds to the outer ring, and R_2 refers to the ring connected to the pyridine group. [b]Dihedral OOOO angle. [c]Dihedral CNCC angles of pyridine (d_2), piperazine (d_3: toward ferrocene; d_4: toward azacrown ether), and azacrown ether (d_5), i.e., dihedral angles of the N atom and its nearby connected C atoms. [d]X = N for W_a, R(N···HOH); X = C of the phenyl group for W_b, R(C···HOH). [e]R(H_2O···H(of the phenyl group)). [f]R(H_2O···H(of the CH_2 group)).

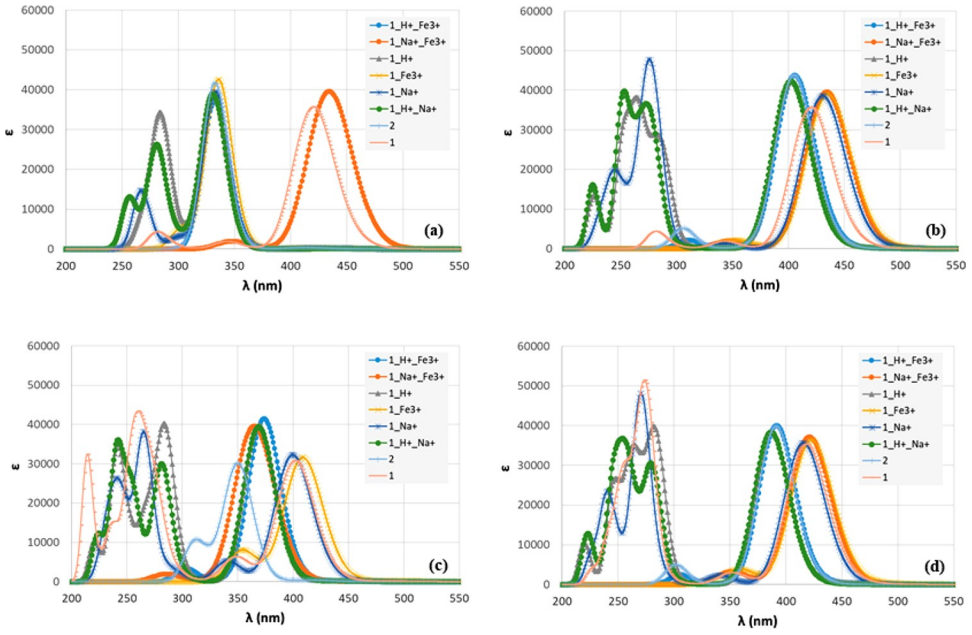

Figure 4. Absorption spectra of the calculated minimum structures: (a) implicit inclusion of a solvent; (b) implicit inclusion of a solvent at the minimum structure of **1-Na$^+$-Fe^{3+}**; (c) implicit inclusion of a solvent and explicit inclusion of a water molecule from the A position; (d) implicit and explicit inclusion of a water molecule from the B position at the PBE0/6-31G(d,p) in the water solvent.

Na$^+$···W_b and **2**···W_b complexes does not affect the geometry of their naphthalimide nitrogen adjacent to the naphthalene which is found to be critical to obtain agreement with experimental data, see below. The CNCC dihedral angles in **1-Na$^+$···3W** and **2···3W** are 152.0 and 150.1 degrees, respectively, i.e., they differ only about 1 degree from the corresponding values of the **1-Na$^+$···W_b** and **2**···W_b complexes.

Thus, we found that the complexation or the oxidation of Fe affects the geometry of remote groups. Additionally, the explicit inclusion of the solvent also alters their geometries, including the geometry of remote groups from the attached water molecules. Below, these geometry changes of the complexes are matched with changes in their spectra and compared with experimental data. The role of specific groups of complexes to the shifts of the peaks is highlighted.

IIIB. Spectrum, Energetics, and Molecular Orbitals. *IIIB1. Absorption Spectra.* The absorption spectra (a) and relative absorbance % spectra (b) of the calculated minimum structures in the water solvent are presented in Figure 4 and Figures S2−S5 of the SI. The λ values with and without cLR

https://doi.org/10.1021/acs.jcim.2c00257
J. Chem. Inf. Model. 2022, 62, 6436−6448

Table 3. Absorption Maxima and Charge Transfer Peaks, λ (nm) and the LR Corrected λ_{CLR} (nm) Values, Energy Differences ΔE (eV) and LR Corrected ΔE_{CLR} (eV) of $S_0 \rightarrow S_x$, *f*-Values, and Corresponding Main Excitations for the Absorption Spectra of the 1, 1-H^+, 1-Na^+, 1-Fe^{3+}, 1-Na^+-Fe^{3+}, 1-H^+-Na^+, 1-H^+-Fe^{3+}, and 2 Species at the PBE0/6-31G(d,p) Level of Theory in the Water Solvent

molec	type[a]	peaks	λ	ΔE	λ_{CLR}	ΔE_{CLR}	*f*	main excitations
1[a]	I	CT	461.6	2.686	655.6	1.891	0.0040	0.999 |H → L>
		main	420.0	2.952	422.8	2.932	0.3932	0.748 |H-3 → L>
	III	CT	484.1	2.561	702.4	1.765	0.0019	0.999 |H → L>
		main	401.4	3.089	408.7	3.034	0.3396	0.989 |H-3 → L>
	IV	CT	471.8	2.628	672.3	1.844	0.0032	0.999 |H → L>
		main	418.3	2.964	421.5	2.942	0.3800	0.876 |H-3 → L>
1-H^+	I	CT	472.9	2.622	689.7	1.798	0.0011	1.000 |H → L>
		main	331.0	3.746	327.8	3.783	0.4385	0.961 |H-5 → L>
	II	CT	421.2	2.944			0.0043	0.998 |H → L>
		main	402.7	3.079			0.4675	0.988 |H-3 → L>
	III	CT	458.9	2.702	648.1	1.913	0.0026	1.000 |H → L>
		main	369.3	3.357	368.3	3.366	0.4426	0.988 |H-3 → L>
	IV	CT	451.8	2.744	630.9	1.965	0.0038	0.999 |H → L>
		main	387.1	3.203	386.7	3.207	0.4282	0.989 |H-3 → L>
1-Na^+	I	CT	436.5	2.840	439.3	2.822	0.0009	0.404 |H → L>
		main	333.6	3.717	332.2	3.733	0.2775	0.680 |H-6 → L> + 0.404 |H-7 → L>
	II	CT	422.5	2.934			0.0233	0.757 |H → L>
		main	431.3	2.874			0.3942	0.822 |H-2 → L>
	III	CT	418.2	2.965	519.7	2.386	0.0030	0.952 |H → L>
		main	399.9	3.101	407.4	3.044	0.3422	0.946 |H-3 → L>
	IV	CT	410.3	3.022	481.5	2.575	0.0407	0.807 |H → L>
		main	416.2	2.979	419.9	2.953	0.3550	0.791 |H-3 → L>
	V	CT	432.3	2.868	524.4	2.364	0.0130	0.798 |H → L>
		main	422.7	2.934	425.2	2.916	0.3965	0.961 |H-2 → L>
1-H^+-Na^+	I	CT	449.5	2.758	568.9	2.179	0.0008	0.993 |H → L>
		main	330.8	3.748	327.6	3.785	0.4319	0.988 |H-4 → L>
	II	CT	446.7	2.776			0.0007	0.774 |H → L>
		main	402.3	3.082			0.4711	0.988 |H-2 → L>
	III	CT	437.1	2.837	479.6	2.585	0.0013	0.773 |H → L>
		main	368.8	3.362	367.8	3.371	0.4354	0.987 |H-3 → L>
	IV	CT	426.5	2.907	532.3	2.329	0.0011	0.944 |H → L>
		main	386.9	3.205	387.2	3.202	0.4195	0.960 |H-3 → L>
1-Na^+-Fe^{3+}	I	CT	682.1	1.818			0.0004	0.988 |H → S>
		main	434.7	2.852	436.8	2.839	0.4281	0.690 |H → L> + 0.569 |S → L+2>
	II	CT	682.1	1.818			0.0004	0.988 |H → S>
		main	434.7	2.852			0.4281	0.690 |H → L> + 0.569 |S → L+2>
	III	CT	625.5	1.982			0.0003	0.991 |H → S>
		main	407.3	3.044	425.1	2.917	0.2867	0.595 |H-1 → L>
	IV	CT	665.6	1.863			0.0003	−0.270 |H → S> + 0.957 |H-1 → S>
		main	421.4	2.942	425.7	2.912	0.3977	0.591 |H → L+2> + 0.667 |H-1 → L>
1-H^+-Fe^{3+}	I	CT	667.5	1.858			0.0001	1.000 |H → S>
		main	332.0	3.734	334.2	3.710	0.3802	0.575 |H-2 → L+1> − 0.544 |H-3 → L>
	II	CT	652.6	1.900			0.0002	1.000 |H → S>
		main	405.8	3.056			0.4634	0.681 |H → L> + 0.682 |H → S>
	III	CT	760.5	1.630			0.0002	1.000 |H → S>
		main	373.8	3.317	373.5	3.320	0.4607	0.700 |H → L> + 0.695 |H-1 → L>
	IV	CT	770.3	1.610			0.0002	1.000 |H → S>
		main	391.6	3.167	392.8	3.156	0.4392	0.690 |H → L> + 0.700 |H-1 → L>
1-Fe^{3+}	I	CT	896.6	1.383			0.0001	1.000 |H → S>
		main	335.9	3.692	335.7	3.693	0.4666	0.693 |H-3 →L> + 0.692 |H-4 →L>
	II	CT	771.3	1.608			0.0002	1.000 |H → S>
		main	435.8	2.845			0.4187	0.693 |H-1 →L>
	III	CT	917.2	1.352			0.0002	1.000 |H → S>
		main	408.8	3.033	417.6	2.969	0.3438	0.697 |H-1 → L>
	IV	CT	898.8	1.379			0.0002	1.000 |H → S>
		main	423.4	2.928	427.7	2.899	0.3920	0.693 |H-1 → L> + 0.627 |H → L+2>
2	I	CT	569.1	2.178			0.0001	1.000 |H → S>
		main	332.7	3.727	331.0	3.746	0.4619	0.551 |H-1 → L> + 0.536 |H→ L>

https://doi.org/10.1021/acs.jcim.2c00257
J. Chem. Inf. Model. 2022, 62, 6436−6448

Table 3. continued

molec	type[a]	peaks	λ	ΔE	λ_{CLR}	ΔE_{CLR}	f	main excitations
	II	CT	637.0	1.946			0.0002	−0.650 |S → L> + 0.656 |H → L>
		CT	577.4	2.147			0.0003	0.971 |H → S>
		main	405.3	3.060			0.4559	0.656 |S → L> + 0.657 |H → L>
	III	CT	569.2	2.178			0.0003	1.000 |H → S>
		main	351.3	3.530	352.7	3.515	0.3095	0.672 |H → L> + 0.669 |H-1 → L>
	IV	CT	580.9	2.134			0.0003	0.989 |H → S>
		main	392.5	3.159	421.4	2.942	0.2515	0.525 |H → L> + 0.489 |S → L> + 0.483 |H-1 → L>
	V	CT	548.9	2.259			0.0000	0.860 |H → S>
		main	398.2	3.114	399.2	3.106	0.4273	0.671 |H → L> + 0.672 |H-1 → L>

[a]**I**: implicit inclusion of a solvent; **II**: implicit inclusion of a solvent at the minimum structure of **1**-Na^+-Fe^{3+}; **III**: implicit inclusion of a solvent and explicit inclusion of a water molecule from the A position; **IV**: implicit and explicit inclusion of a water molecule from the B position. **V**: implicit and explicit inclusion of three water molecules, one of them from the B position.

correction are given in Table 3. Note that the LR correction slightly affects the main peaks. The largest shift is 29 nm for **2** with the explicit inclusion of a water molecule. It is theoretically found that the main peaks in the visible area of the minimum structures are observed only for **1** and **1**-Na^+-Fe^{3+} at 423 and 437 nm, respectively, when the water molecule is added only implicitly via the dielectric constant, in disagreement with the experiment where the main peaks of all eight structures are around 400 nm. Note that these molecules present d_3 CNCC angles (N atom of piperazine toward the ferrocene) at 151.1 and 158.8 degrees, while the remaining complexes have d_3 dihedral angles of 142−146 degrees, and their main peak is about 330 nm, Figure 4. With freezing of the d_3 dihedral angle at 158.8, the corresponding absorption spectra of all structures obtained are shown in Figure 4b, and all peaks are at about 430 nm, i.e., some of the peaks are red-shifted up to 100 nm with respect to the peaks in their global minimum. The same red shifts are obtained when a water molecule is added nearby this N atom, i.e., there are red shifts up to 92 nm, resulting in all main peaks to be found in the visible area, around 410 nm. Finally, the **1**-Na^+···**3W** and **2**···**3W** complexes, where three water molecules are included explicitly in addition to the explicit solvent, also present main peaks around 400 nm in agreement with the experimental values. Note that their CNCC dihedral angles, which are critical to obtain agreement with experimental data, are about 150 degrees, i.e., they are similar to the dihedral angles of all species including one water molecule from the "a" or "b" direction.

Thus, either all species are geometry optimized including a water molecule next to the N atom of piperazine, or they have a fixed d_3 dihedral angle as the corresponding one of **1**-Na^+-Fe^{3+}. Now, all structures present a main peak in the visible area range from 387(387) nm (**1**-H^+) to 423(428) nm (**1**-Fe^{3+}), while similar values at 416(420) nm and 421(426) nm are obtained for **1**-Na^+ and **1**-Na^+-Fe^{3+}, respectively, without-(with) cLR correction. These values are in excellent agreement with the experimental values of the peaks of the absorption spectra that range from 390 nm (**1**-H^+) to 415 nm (**1**-Na^+, **1**-Fe^{3+}, **1**-Na^+-Fe^{3+}) nm in the MeOH/H_2O solvent.[18] Finally, all species have similar oscillator strengths for their main peak, i.e., the height of the peaks is similar. This is observed both theoretically and experimentally, except for **1**-Na^+ which has been experimentally observed to have a smaller peak by 25% compared to the other species. All of the above show the importance of the geometry of the N atom of piperazine. Its geometry or its environment is the key for the correct calculation of the absorption spectra of the complexes. Finally, it should be noted that the addition of a water molecule next to the other group of the molecule does not result in any significant shifts of the main peak in the absorption spectra.

Regarding the first excited states, all are charge transfer states (CT) for all eight molecular structures, with and without the explicit inclusion of water. Unlike with main peaks, the CT peaks are significantly shifted to smaller energy values when the LR correction is applied. The red shifts range from 4 nm (**1**-Na^+) to 218 (**1**) nm, showing that the cLR large nonequilibrium effects for some CT excitations are very significant, meaning that the dynamical response of the solvent needs to be equilibrated with the excited state density, and thus, the LR correction should be examined for CT excitations of the absorption spectrum. The first excited states (CT peaks) are observed in λ values ranging from 420 nm (**1**-Na^+) to 672 nm (**1**) when the iron is Fe^{2+}. When the iron is oxidized, the CT states including LR corrections do not converge due to technical issues and may be due to the open-shell nature of the Fe^{3+} cation which may influence the CT processes. The uncorrected CT peak of **1**-Fe^{3+} is in the near-IR area, while the peaks of the remaining structures are at 581 nm (**2**), 666 nm (**1**-Na^+-Fe^{3+}), and 770 nm (**1**-H^+-Fe^{3+}, in near-IR).

Finally, all have peaks of high intensity in the UV area, see Figure 4 and Figures S1−S4 of the SI. Their intensity is as high as the intensity of the main peak in the visible area. In all cases, there are two peaks around 270 nm, i.e., they range from 266.5 to 280.0 nm, and around 245 nm, i.e., they range from 241.2 to 255.2 nm, see Table 4 and Table S6 of the SI.

IIIB2. Emission Spectra. A notable fluorescence emission is found for **2** when all three inputs are simultaneously present (H^+, Na^+, Fe^{3+}) in excellent accordance with the experimental

Table 4. Absorption Maxima in UV Area λ (nm) Values, Energy Differences ΔE (eV), and f-Values of the 1, 1-H^+, 1-Na^+, and 1-H^+-Na^+ at the PBE0/6-31G(d,p) Level of Theory in the Water Solvent Adding a Water Molecule Explicitly

	ΔE	λ	f
1	4.500	275.5	0.2186
	4.858	255.2	0.1538
1H^+	4.395	282.1	0.1527
	5.046	245.7	0.2643
1-Na^+	4.576	271.0	0.3251
	5.141	241.2	0.1619
1-H^+-Na^+	4.428	280.0	0.2891
	4.786	259.0	0.1680

https://doi.org/10.1021/acs.jcim.2c00257
J. Chem. Inf. Model. 2022, 62, 6436−6448

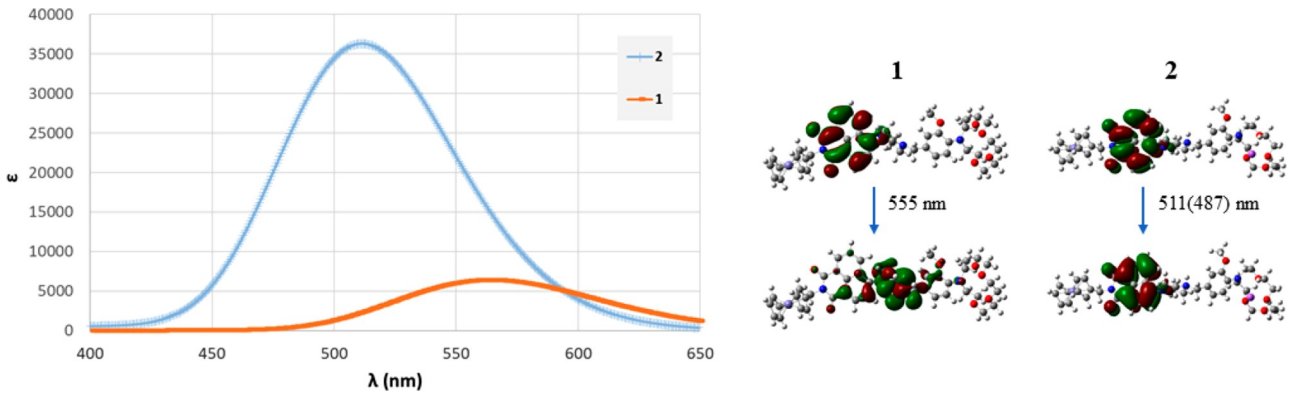

Figure 5. Emission spectra of **2** and **1** calculated minimum structures (left). Electron density plots of the molecular orbitals involved in the excitations and emission maxima without(with) the cLR correction (right).

Table 5. Emission Maxima, λ (nm) and the LR Corrected λ_{CLR} (nm) Values, Energy Differences ΔE (eV) and LR Corrected ΔE_{CLR} (eV) of $S_0 \rightarrow S_x$, *f*-Values, and Corresponding Main Excitations for the Absorption Spectrum of the 1 and 2 Species at the PBE0/6-31G(d,p) Level of Theory in the Water Solvent

molecule	type	λ	ΔE	λ_{CLR}	ΔE_{CLR}	*f*	main excitations
1	I	554.8	2.235			0.115	0.870|H-1 → L>
2	I	384.1	3.228	370.2	3.349	0.515	0.996 |H → L>
	IV	511.4	2.424	487.1	2.545	0.538	0.892 |H → L>
	expt	536	2.313				

finding of Scerri et al.[18] The *f*-value of **2**, i.e., 0.54, is 5 times larger than the *f*-value of **1**, i.e., 0.11, while for the six remaining structures it is less than 0.1. This happens because the emission of **1** has a charge transfer character, as is also the case for the remaining six complexes, where one or two inputs are absent, and the ICT pathway adequately deactivates the fluorescent excited state. On the contrary, in **2**, this emission peak corresponds to a peak where the electron density remains with the naphthalimide fluorophore, see Figure 5. It should be noted that, experimentally, it was found that all seven species **1**, **1-M**, and **1-M1-M2** have the same emission spectra.[18] Here, it is found that **1** presents a small peak with $f = 0.11$, while the remaining six **1-M** and **1-M1-M2** complexes have a significantly lower emission peak. This has been examined further. Several excited states next to the state that provides the main peak in the absorption spectrum have been geometry optimized; however, all emitted structures result in an emitting peak with $f < 0.1$. The only explanation is that the computation of quenched emitting states of electron charged structures, i.e., due to the existence of H^+, Na^+, and Fe^{3+}, may lead to more intense quenching of the emitting state. However, even though there is a small difference between experimental and theoretical data regarding the intensity of the quenching of the emitting state between **1** and **1-M** and **1-M1-M2**, it is clearly found that **2** has a significantly larger *f*-value than the remaining seven species, i.e., **2** has an enhanced emission peak, in excellent agreement with the experimental data.

The emission of **2** is calculated at 511 nm in very good agreement with the experimental value of 536 nm. **1** presents an emitting peak in this area, 555 nm, see Figure 5, in excellent agreement with the experimental spectra,[18] see Table 5. The LR correction causes only a small red shift of about 0.1 eV (20 nm). Note that a water molecule was necessary to include in the calculation again. Without the inclusion of the water molecule, the peak was blue-shifted by about 130 nm (0.8 eV), but it retains its high intensity. Finally, it should be noted that the six **1-M** and **1-M1-M2** complexes have emission peaks with very small *f*-values in the area around 500 nm; thus, it is not possible to choose which one is the exact value of the emitting peak.

The energy differences of the adjacent highest occupied orbitals in the emitting state of **1** are 0.004 eV (H-3 and H-2), 0.41 eV (H-2 and H-1), and 0.37 eV (H-1 and H), while in **2**, the energy differences are 0.07 eV (H-2 and H-1), 0.24 eV (H-1 and H), and 0.75 eV (H and S). The H → L excitation in **1** is 2.51 eV, while in **2**, the S → L and H → L excitations are 3.10 and 3.85 eV. Thus, the energy differences of the four lowest occupied orbitals H-3 up to H are within 0.78 eV, while in **2**, the four lowest occupied orbitals H-2 up to S are within 1.82 eV, showing that they are more distant in energy. The existence of occupied orbitals with similar energies in **1** may assist the quenching process. Additionally, the energy differences of the occupied orbitals of piperazine and naphthalimide are slightly larger in **2** than the remaining seven species, which is indicative of the CT character of the emission being enhanced in the seven species. Finally, in **2**, the simultaneous presence of H^+, Na^+, and Fe^{3+} helps to delocalize the electron density from the piperazine, and thus, the main peak of the emission spectra corresponds to a peak where the electron density remains in the fluorophore.

IIIB3. Molecular Orbitals. The frontier molecular orbitals are shown in Figures 6 and 7. For the Fe^{2+} complexes, when the solvent is added only implicitly, the HOMO → LUMO (H→L) excitations are charge transfer excitations from the ferrocene group to the naphthalimide group, i.e., to the fluorophore. It is also interesting that, in this case, the main peak is also a CT excitation from ferrocene (**1**) or the phenyl-crown ether (**1-H$^+$**) or piperazine (**1-H$^+$-Na$^+$**) to the naphthalimide group. When the solvent is added implicitly and explicitly, the H→L excitations are again charge transfer excitations with the same character as above for **1-Na$^+$** and **1-H$^+$-Na$^+$**, while for **1** and **1-H$^+$**, the CT excitation is from the

https://doi.org/10.1021/acs.jcim.2c00257
J. Chem. Inf. Model. 2022, 62, 6436−6448

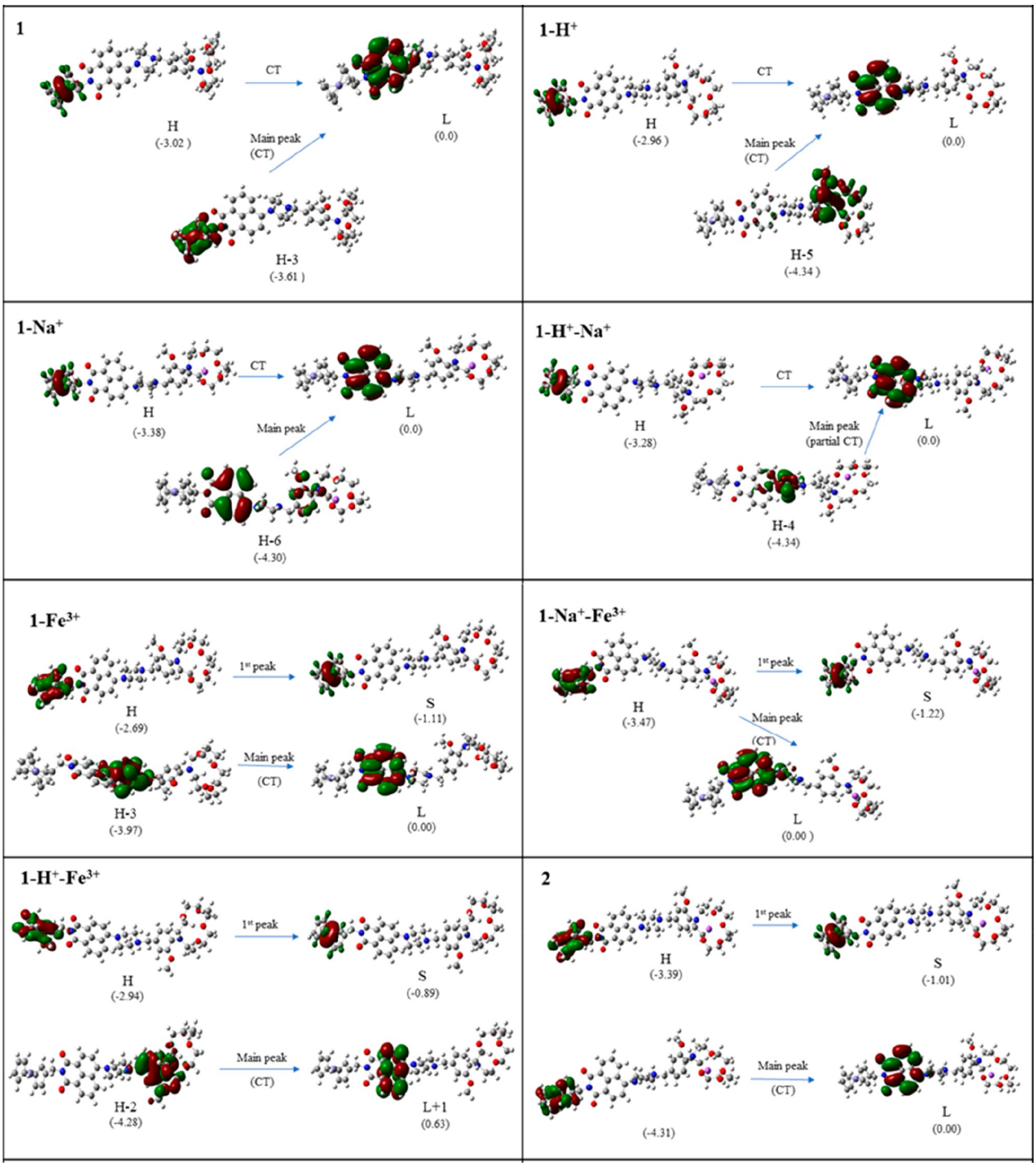

Figure 6. Electron density plots of the molecular orbitals involved in the excitations corresponding to the major and the first CT peaks of the calculated minimum structures at the PBE0/6-31G(d,p) in the water solvent. Their relative energies of MO are given in eV.

phenyl-crown ether group to the fluorophore. However, the main peak, which is now in the visible area for all four complexes, is not a CT excitation. Thus, the explicit addition of the solvent affects both the absorption peaks and their character.

For the Fe^{3+} complexes, when the solvent is added only implicitly, the HOMO → SOMO (H→S) excitations are not CT excitations, and the electron density remains to ferrocene. On the contrary, the main peak has a CT character, and the electron density is transferred from piperazine (**1-Fe^{3+}**, **1-H^{+}-Fe^{3+}**) or ferrocene (**1-Na^{+}-Fe^{3+}**, **2**) to the fluorophore. However, when the solvent is added implicitly and explicitly, H→S excitation is a CT excitation from the phenyl-crown ether to ferrocene. Note that, with or without explicit inclusion of the solvent, the electron density is located on the ferrocene in the S orbital. In all cases, the main peak in the visible area corresponds to excitation, where the electron density is located on the fluorophore.

Thus, we conclude that the explicit inclusion of a solvent molecule next to the key atom (N of piperazine) can change

https://doi.org/10.1021/acs.jcim.2c00257
J. Chem. Inf. Model. 2022, 62, 6436−6448

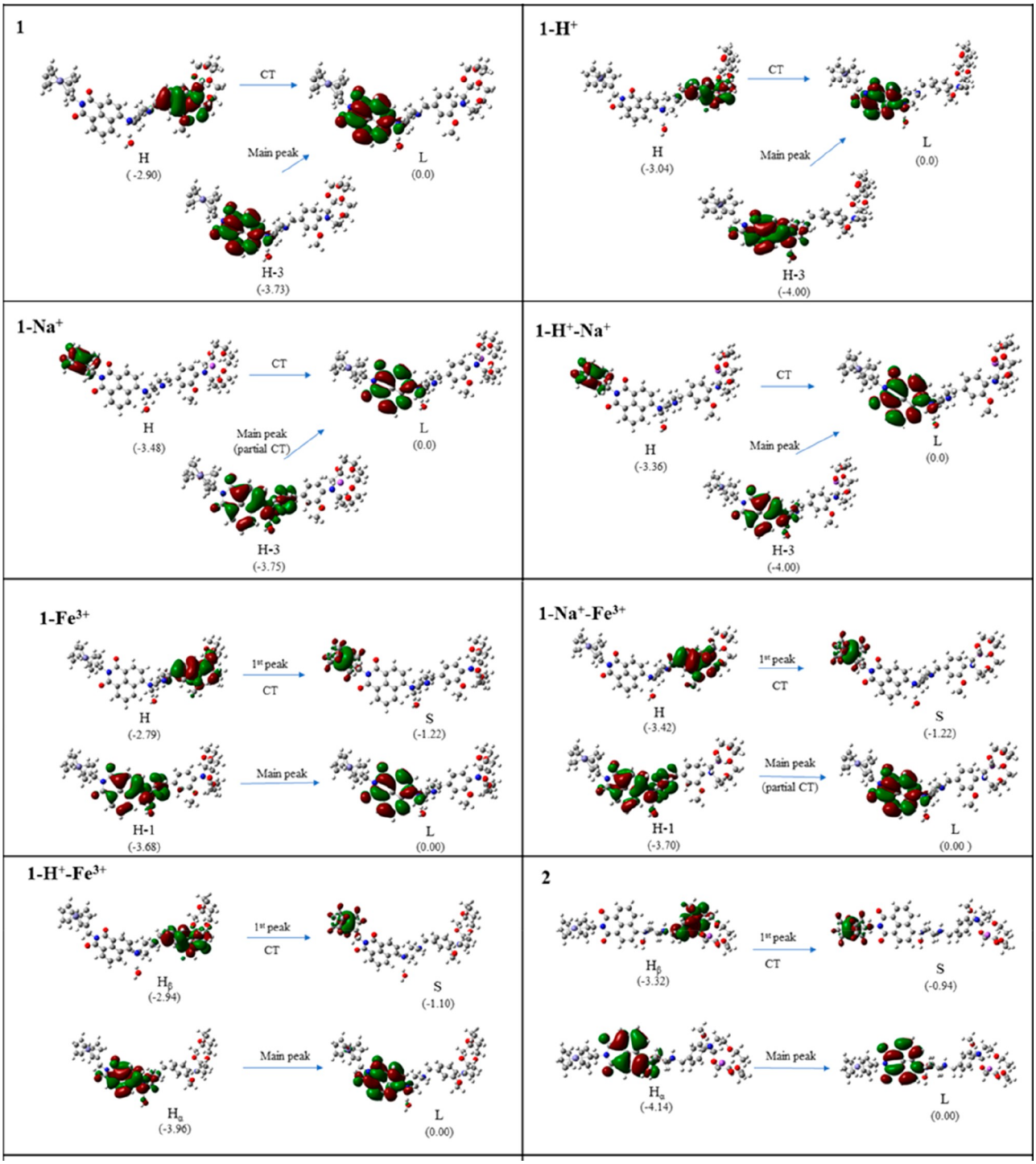

Figure 7. Electron density plots of the molecular orbitals involved in the excitations corresponding to the major and the first CT peaks of the calculated minimum structures including a water molecule explicitly from the A position at the PBE0/6-31G(d,p) in the water solvent. Their relative energies of MO are given in eV.

the character of the main peaks, for instance, without the water molecule, the main peak is a charge transfer state for most of the complexes, while when the water is added explicitly, this is altered. However, with or without the explicit inclusion of the water molecule, when the main peak is calculated in the visible area, it corresponds to an excited state where the electron density is located in the fluorophore, showing that the type of excitation, i.e., CT or not, goes hand-in-hand with the area of absorbance. It is found that, for all Fe^{3+} complexes, the SOMO orbital has the electron density located on ferrocene. To conclude, the addition of the water is necessary not only because it predicts the experimentally measured peaks correctly but also because the observation of a main peak with a CT character is not common, and this is a clue that something is missing from the evaluation of the complexes.

IIIB4. Oxidation of Iron Cation: $Fe^{2+} \rightarrow Fe^{3+}$. The Fe^{2+} complexes are more stable than the Fe^{3+} by about 5.1 eV in all complexes (Table 6), either including explicitly a water

https://doi.org/10.1021/acs.jcim.2c00257
J. Chem. Inf. Model. 2022, 62, 6436−6448

Table 6. Oxidation Energy $Fe^{2+} \rightarrow Fe^{3+}$ in the Calculated Complexes in eV

oxidation	in solvent	in solvent + W_a	in solvent + W_b
$1 \rightarrow 1 + Fe^{3+}$	5.606	5.119	5.112
$1+H^+ \rightarrow 1+H^++Fe^{3+}$	5.106	5.140	5.135
$1+Na^+ \rightarrow 1+Na^++Fe^{3+}$	5.095	5.128	5.091
$1+H^++Na^+ \rightarrow 2$	5.115	5.161	5.145
$Fe^{2+} \rightarrow Fe^{3+}$	30.968		
RCCSD(T)/AVTZ[a]	30.10		
expt[b]	30.651		

[a]Reference 31. [b]Reference 32.

molecule or not. It should be noted that our methodology predicts very well the atomic $Fe^{2+} \rightarrow Fe^{3+}$ oxidation in excellent agreement with the RCCSD(T)/AVTZ value of 30.10 eV[31] and the experimental value of 30.651 eV.[32] It has been reported that the complexation stabilizes the Fe^{3+} complexes significantly. Moreover, the ionic bonds between iron and ligands result in larger stabilization than the covalent bonds. Furthermore, in some cases, for instance, in $[Fe(SCH_3)_4]^{2-/-}$ complexes, Fe^{3+} can form more stable complexes than Fe^{2+}.[31] Here, the oxidation energy of 5.1 eV (= 243 nm) corresponds to the excitations at the UV area of the absorption spectra with high oscillator strength, showing that the energy excitation at about the 35th singlet excited state and the oxidation of Fe^{2+} are two contradictory processes. The main peaks in this case are found in 4.86 eV (**1**), 5.05 eV (**1**-H^+), 5.14 eV (**1**-Na^+), and 4.79 eV (**1**-H^+-Na^+), see Table 6.

4. SUMMARY AND CONCLUSIONS

Here, we study theoretically, via DFT and TD-DFT calculations, the photophysical properties of a 3-input AND molecular logic gate which has the 'electron donor-spacer-fluorophore−spacer−receptor1−spacer−receptor2' format, and it presents an enhanced fluorescence spectrum. All eight species involved in the logical operation are studied. The unusually enhanced fluorescence of **2** in contrast to the remaining seven molecular species is explained, while the key factors for the accurate prediction of their absorption spectra are found and analyzed.

It is found that the complexation, protonation, and the oxidation of Fe in **1** affects the geometry of remote groups. Additionally, the explicit inclusion of the solvent also alters the geometry of remote groups from the attached water molecules. These geometrical changes of the complexes are matched with changes in their spectra.

The calculated molecules have four N atoms. The geometry of one of them, i.e., the N atom of piperazine connected to naphthalimide, is the key factor for the correct calculation of the spectra of all eight molecular species, since it is expected to control the degree of π-electron delocalization. This atom has a geometry between tetrahedral and planar, around 140−158 degrees. Changes in its geometry (CNCC dihedral angle, d_3) of about 10 degrees can cause significant shifts of the main peak of the absorption spectra up to 100 nm.

Regarding the absorption spectrum, the explicit inclusion of one or three water molecules next to this N atom of piperazine or the fixed d_3 dihedral angle at about 150 degrees results in a main peak in the visible area that ranges from 387(387) nm to 423(428) nm, without(with) LR correction, in excellent agreement with the experimental values that range from 390 to 415 nm in the MeOH/H_2O solvent.[18] Both theoretically and experimentally, the highest energy peak (blue-shifted) is found for **1**-H^+, while the lowest energy peaks (red-shifted) are found for **1**-Na^+, **1**-Fe^{3+}, and **1**-Na^+-Fe^{3+}, which differ by less than 7 nm. Finally, all species have similar oscillator strengths for their main peak, i.e., the intensity of the peaks is similar. This is observed both theoretically and experimentally, except for **1**-Na^+ which has been experimentally observed to have a smaller peak by 25% compared to the other species. All of the above show the importance of the N atom of piperazine connected to naphthalimide, i.e., its geometry and/or its environment is the key factor for the correct calculation of the absorption spectra of the complexes.

2 is a 3-input AND MLG because it has an enhanced fluorescence emission in excellent accordance with the experimental findings.[18] The *f*-value of **2** is at least 5 times larger than the *f*-value of the remaining seven species. This happens because the emission of all species, apart from **2**, has a charge transfer character because their highest occupied orbitals of piperazine and naphthalimide are energetically degenerate, and thus, the ICT pathway adequately deactivates the fluorescent excited state. On the contrary, the emission peak of **2** corresponds to a peak where the electron density remains on the fluorophore (naphthalimide), and it is calculated at 511 nm in very good agreement with the experimental value of 536 nm. Finally, **1** presents a small emitting peak in this area, 555 nm, also in excellent agreement with experimental spectra.[18]

The Fe^{2+} complexes are more stable than the Fe^{3+} by about 5.1 eV (= 243 nm). This oxidation energy corresponds to the main peak excitations of the absorption spectra at the UV area of the calculated complexes of Fe^{2+}, i.e., 4.86 eV (**1**), 5.05 eV (**1**-H^+), 5.14 eV (**1**-Na^+), and 4.79 eV (**1**-H^+-Na^+), showing that the energy excitation of the complexes and the oxidation of Fe^{2+} are two contradictory processes.

It has been shown that the flexibility of the geometry of N atoms can be related to the quenching or not of the emission spectrum.[13,14,30] This is the key for the prediction of the fluorescence sensors and molecular logic gates. Thus, molecular systems having N atoms, whose geometry in the lowest in the energy state is between planar and tetrahedral, can be ideal molecules as sensors and molecular logic gates. Furthermore, attention should be paid to the accurate calculation of the spectra of the molecules having such N atoms. The explicit inclusion of the solvent next to them can be necessary, even in the cases where no direct interactions are formed.

5. DATA AND SOFTWARE AVAILABILITY

The data that support the findings of this study are available within the article and its Supporting Information.

■ ASSOCIATED CONTENT

Supporting Information

The Supporting Information is available free of charge at https://pubs.acs.org/doi/10.1021/acs.jcim.2c00257.

Geometry, energetics, molecular orbitals, absorption spectra, and relative absorbance % spectra of calculated structures (PDF)

https://doi.org/10.1021/acs.jcim.2c00257
J. Chem. Inf. Model. 2022, 62, 6436−6448

AUTHOR INFORMATION

Corresponding Author

Demeter Tzeli − *Laboratory of Physical Chemistry, Department of Chemistry, National and Kapodistrian University of Athens, Athens 157 84, Greece; Theoretical and Physical Chemistry Institute, National Hellenic Research Foundation, Athens 116 35, Greece;* orcid.org/0000-0003-0899-7282; Phone: +30-210-727-4307; Email: tzeli@chem.uoa.gr

Author

Christina Eleftheria Tzeliou − *Laboratory of Physical Chemistry, Department of Chemistry, National and Kapodistrian University of Athens, Athens 157 84, Greece*

Complete contact information is available at: https://pubs.acs.org/10.1021/acs.jcim.2c00257

Notes

The authors declare no competing financial interest.

ACKNOWLEDGMENTS

We acknowledge the National and Kapodistrian University of Athens, Special Accounts for Research Grants for supporting of this research through the project "SONFM" (KE 17034). The authors support advancing women in chemistry.

REFERENCES

(1) de Silva, A. P.; Gunaratne, H. Q. N.; McCoy, C. P. A molecular photoionic AND gate based on fluorescent signalling. *Nature* **1993**, *364*, 42−44.

(2) Tzeli, D.; Petsalakis, I. D.; Theodorakopoulos, G. Molecular logic gates based on benzo-18-crown-6 ether of styrylquinoline: a theoretical study. *Phys. Chem. Chem. Phys.* **2016**, *18*, 32132−32145.

(3) Wang, B.; Buck, M. Rapid engineering of versatile molecular logic gates using heterologous genetic transcriptional modules. *Chem. Commun.* **2014**, *50*, 11642−11644.

(4) Núñez, C.; Santos, S. M.; Oliveira, E.; Santos, H. M.; Capelo, J. L.; Lodeiro, C. Rhodamine-appended bipyridine: XOR and OR logic operations integrated in an example of controlled metal migration. *ChemistryOpen* **2014**, *3*, 190−198.

(5) Erbas-Cakmak, S.; Kolemen, S.; Sedgwick, A. C.; Gunnlaugsson, T.; James, T. D.; Yoon, J.; Akkaya, E. U. Molecular logic gates: the past, present and future. *Chem. Soc. Rev.* **2018**, *47*, 2228.

(6) Sreejith, S.; Ajayaghosh, A. Molecular logic gates: Recent advances and perspectives. *Indian J. Chem.* **2012**, *51A*, 47−56.

(7) Kumar, A.; Kumar, S.; Chae, P. S. A novel anthrapyridone diamine-based probe for selective and distinctive Cu^{2+} and Hg^{2+} sensing in aqueous solution; utility as molecular logic gates. *Dyes Pigm.* **2020**, *181*, 108522.

(8) Stojanovic, M. N.; Mitchell, T. E.; Stefanovic, D. Deoxyribozyme-Based Logic Gates. *J. Am. Chem. Soc.* **2002**, *124*, 3555−3561.

(9) Yan, G. T.; Li, H.; Zhu, Y. R.; Shi, B. B.; Qu, W.; Lin, Q.; Yao, H.; Zhang, Y. M.; Wei, T. B. A highly selective colorimetric and "Off-On" fluorescent chemosensor for fluoride ions and its application as a molecular-scale logic device. *New J. Chem.* **2015**, *39*, 8797−8801.

(10) Coskun, A.; Deniz, E.; Akkaya, E. U. Effective PET and ICT switching of boradiazaindacene emission: A unimolecular, emission-mode, molecular half-subtractor with reconfigurable logic gates. *Org. Lett.* **2005**, *7*, 5187−5189.

(11) Mano, M. M.; Kime, C. R. *Logic and Computer Design Fundamentals*, 4th ed.; Pearson Education Limited: 2014.

(12) Ling, J.; Daly, B.; Silverson, V. A. D.; de Silva, A. P. Taking baby steps in molecular logic-based computation. *Chem. Commun.* **2015**, *51*, 8403−8409.

(13) Tzeli, D.; Petsalakis, I. D.; Theodorakopoulos, G. Theoretical study of the photophysical processes of a styryl-bodipy derivative eliciting an AND molecular logic gate response. *Int. J. Quantum Chem.* **2019**, *119*, No. e25958.

(14) Tzeli, D.; Petsalakis, I. D.; Theodorakopoulos, G. The solvent effect on a styryl-bodipy derivative functioning as an AND molecular logic gate. *Int. J. Quantum Chem.* **2020**, *120*, No. e26181.

(15) Bozdemir, O. A.; Guliyev, R.; Buyukcakir, O.; Selcuk, S.; Kolemen, S.; Gulseren, G.; Nalbantoglu, T.; Boyaci, H.; Akkaya, E. U. Selective manipulation of ICT and PET Processes in styryl-Bodipy derivatives: applications in molecular logic and fluorescence sensing of metal ions. *J. Am. Chem. Soc.* **2010**, *132*, 8029−8036.

(16) Magri, D. C. Logical sensing with fluorescent molecular logic gates based on photoinduced electron transfer. *Coord. Chem. Rev.* **2021**, *426*, 213598.

(17) (a) Spiteri, J. C.; Denisov, S. A.; Jonusauskas, G.; Klejna, S.; Szaciłowski, K.; McClenaghan, N. D.; Magri, D. C. Molecular engineering of logic gate types by module rearrangement in 'Pourbaix Sensors': the effect of excited-state electric fields. *Org. Biomol. Chem.* **2018**, *16*, 6195−6201. (b) Scerri, G. J.; Cini, M.; Schembri, J. S.; da Costa, P. F.; Johnson, A. D.; Magri, D. C. Redox-Enabled, pH-Disabled Pyrazoline-Ferrocene INHIBIT Logic Gates. *ChemPhysChem* **2017**, *18*, 1742−1745. (c) Refalo, M. V.; Farrugia, N. V.; Johnson, A. D.; Klejna, S.; Szaciłowski, K.; Magri, D. C. Fluorimetric naphthalimide-based polymer logic beads responsive to acidity and oxidisability. *J. Mater. Chem. C* **2019**, *7*, 15225−15232. (d) Zerafa, N.; Cini, M.; Magri, D. C. Molecular engineering of 1,3,5-triaryl-2-pyrazoline fluorescent logic systems responsive to acidity and oxidisability and attachment to polymer beads. *Mol. Syst. Des. Eng.* **2021**, *6*, 93−99.

(18) Scerri, G. J.; Spiteri, J. C.; Mallia, C. J.; Magri, D. C. A lab-on-a-molecule with an enhanced fluorescent readout on detection of three chemical species. *Chem.Comm.* **2019**, *55*, 4961−4964.

(19) Ma, X.; Chen, X.; Tang, Y.; Yan, R.; Miao, P. Triple-Input Molecular AND Logic Gates for Sensitive Detection of Multiple miRNAs. *ACS Appl. Mater. Interfaces* **2019**, *11*, 41157−41164.

(20) Hettie, K. S.; Klockow, J. L.; Glass, T. E. Three-Input Logic Gates with Potential Applications for Neuronal Imaging. *J. Am. Chem. Soc.* **2014**, *136*, 4877−4880.

(21) Lin, J.-H.; Tseng, W.-L. Design of two and three input molecular logic gates using non-Watson-Crick base pairing-based molecular beacons. *Analyst* **2014**, *139*, 1436−1441.

(22) Lederman, H.; Macdonald, J.; Stefanovic, D.; Stojanovic, M. N. Deoxyribozyme-based three-input logic gates and construction of a molecular full adder. *Biochemistry* **2006**, *45*, 1194−1199.

(23) (a) Perdew, J. P.; Burke, K.; Ernzerhof, M. Generalized Gradient Approximation Made Simple. *Phys. Rev. Lett.* **1996**, *77*, 3865. (b) Ernzerhof, M.; Scuseria, G. E. Assessment of the Perdew-Burke-Ernzerhof exchange-correlation functional. *J. Chem. Phys.* **1999**, *110*, 5029. (c) Adamo, C.; Barone, V. Toward reliable density functional methods without adjustable parameters: The PBE0 model. *J. Chem. Phys.* **1999**, *110*, 6158.

(24) (a) Becke, A. D. Density-functional thermochemistry. III. The role of exact exchange. *J. Chem. Phys.* **1993**, *98*, 5648−5652. (b) Lee, C.; Yang, W.; Parr, R. G. Development of the Colle-Salvetti correlation-energy formula into a functional of the electron density. *Phys. Rev. B* **1988**, *37*, 785−789. (c) Vosko, S. H.; Wilk, L.; Nusair, M. Accurate spin-dependent electron liquid correlation energies for local spin density calculations: a critical analysis. *Can. J. Phys.* **1980**, *58*, 1200−1211. (d) Stephens, P. J.; Devlin, F. J.; Chabalowski, C. F.; Frisch, M. J. Ab Initio Calculation of Vibrational Absorption and Circular Dichroism Spectra Using Density Functional Force Fields. *J. Phys. Chem.* **1994**, *98*, 11623−11627.

(25) Curtiss, L. A.; McGrath, M. P.; Blaudeau, J.-P.; Davis, N. E.; Binning, R. C., Jr; Radom, L. Extension of Gaussian-2 theory to molecules containing third-row atoms Ga-Kr. *J. Chem. Phys.* **1995**, *103*, 6104−6113.

(26) (a) Miertuš, S.; Scrocco, E.; Tomasi, J. Electrostatic interaction of a solute with a continuum. A direct utilizaion of AB initio molecular potentials for the prevision of solvent effects. *Chem. Phys.* **1981**, *55*, 117−129. (b) Tomasi, J.; Mennucci, B.; Cammi, R. Quantum

Mechanical Continuum Solvation Models. *Chem. Rev.* **2005**, *105*, 2999−3094.
(27) (a) Caricato, M.; Mennucci, B.; Tomasi, J.; Ingrosso, F.; Cammi, R.; Corni, S.; Scalmani, G. Formation and relaxation of excited states in solution: A new time dependent polarizable continuum model based on time dependent density functional theory. *J. Chem. Phys.* **2006**, *124*, 124520. (b) Guido, C. A.; Caprasecca, S. *How to Perform Corrected Linear Response Calculations in G09*; Dipartimento di Chimica e Chimica Industriale, Università di Pisa: Pisa, 2016; DOI: 10.13140/RG.2.1.1903.7845.
(28) Tzeli, D.; Petsalakis, I. D.; Theodorakopoulos, G. Electronic structure and absorption spectra of supramolecular complexes of a fullerene azacrown ether with a π-extended TTF derivative. *Phys. Chem. Chem. Phys.* **2011**, *13*, 11965−11975.
(29) Frisch, M. J.; Trucks, G. W.; Schlegel, H. B.; Scuseria, G. E.; Robb, M. A.; Cheeseman, J. R.; Scalmani, G.; Barone, V.; Petersson, G. A.; Nakatsuji, H.; Li, X.; Caricato, M.; Marenich, A. V.; Bloino, J.; Janesko, B. G.; Gomperts, R.; Mennucci, B.; Hratchian, H. P.; Ortiz, J. V.; Izmaylov, A. F.; Sonnenberg, J. L.; Williams-Young, D.; Ding, F.; Lipparini, F.; Egidi, F.; Goings, J.; Peng, B.; Petrone, A.; Henderson, T.; Ranasinghe, D.; Zakrzewski, V. G.; Gao, J.; Rega, N.; Zheng, G.; Liang, W.; Hada, M.; Ehara, M.; Toyota, K.; Fukuda, R.; Hasegawa, J.; Ishida, M.; Nakajima, T.; Honda, Y.; Kitao, O.; Nakai, H.; Vreven, T.; Throssell, K.; Montgomery, J. A., Jr.; Peralta, J. E.; Ogliaro, F.; Bearpark, M. J.; Heyd, J. J.; Brothers, E. N.; Kudin, K. N.; Staroverov, V. N.; Keith, T. A.; Kobayashi, R.; Normand, J.; Raghavachari, K.; Rendell, A. P.; Burant, J. C.; Iyengar, S. S.; Tomasi, J.; Cossi, M.; Millam, J. M.; Klene, M.; Adamo, C.; Cammi, R.; Ochterski, J. W.; Martin, R. L.; Morokuma, K.; Farkas, O.; Foresman, J. B.; Fox, D. J. *Gaussian 16, Revision C.01*; Gaussian, Inc.: Wallingford, CT, 2016.
(30) Tzeli, D.; Mercouris, T.; Theorodakopoulos, G.; Petsalakis, I. D. Time-evolution study of photoinduced charge-transfer in tertiary amine-fluorophore systems. *Comp. Theor. Chem.* **2017**, *1115*, 197−207.
(31) Tzeli, D.; Raugei, S.; Xantheas, S. S. Quantitative Account of the Bonding Properties of a Rubredoxin Model Complex $[Fe(SCH_3)_4]^q$, q = −2, −1, + 2, + 3. *J. Chem. Theory Comput.* **2021**, *17*, 6080−6091.
(32) Sugar, J.; Corliss, C. Atomic Energy Levels of the Iron-Period Elements: Potassium through Nickel. *J. Phys. Chem.* **1985**, *14* (Suppl. 2), 1−664.

https://doi.org/10.1021/acs.jcim.2c00257
J. Chem. Inf. Model. 2022, 62, 6436−6448